Quantum dots embedded into silicon nanowires effectively partition electron confinement

Cite as: J. Appl. Phys. **104**, 054305 (2008); https://doi.org/10.1063/1.2973464
Submitted: 15 May 2008 . Accepted: 23 June 2008 . Published Online: 08 September 2008

Pavel V. Avramov, Dmitri G. Fedorov, Pavel B. Sorokin, Leonid A. Chernozatonskii, and Sergei G. Ovchinnikov

Quantum dots embedded into silicon nanowires effectively partition electron confinement

Pavel V. Avramov,[1,a)] Dmitri G. Fedorov,[2] Pavel B. Sorokin,[3,4,5]
Leonid A. Chernozatonskii,[5] and Sergei G. Ovchinnikov[3,4]
[1]*Fukui Institute For Fundamental Chemistry, Kyoto University, 34-3 Takano Nishihiraki, Sakyo, Kyoto 606-8103, Japan*
[2]*Research Institute for Computational Science, National Institute of Advanced Industrial Science and Technology (AIST), Tsukuba, 305-8568, Japan*
[3]*L.V. Kirensky Institute of Physics SB RAS, 660036 Krasnoyarsk, Russian Federation*
[4]*Siberian Federal University, 79 Svobodny Av., 660041 Krasnoyarsk, Russian Federation*
[5]*N.M. Emanuel Institute of Biochemical Physics of RAS, 119334 Moscow, Russian Federation*

(Received 15 May 2008; accepted 23 June 2008; published online 8 September 2008)

Motivated by the experimental discovery of branched silicon nanowires, we performed theoretical electronic structure calculations of icosahedral silicon quantum dots embedded into pentagonal silicon nanowires. Using the semiempirical method, we studied the quantum confinement effect in the fully optimized embedded structures. It was found that (a) the band gaps of the embedded structures are closely related to the linear sizes of the longest constituting part rather than to the total linear dimension and (b) the discovered atypical quantum confinement with a plateau and a maximum can be attributed to the substantial interactions of near Fermi level electronic states of the quantum dots and nanowire segments. © *2008 American Institute of Physics*.
[DOI: 10.1063/1.2973464]

I. INTRODUCTION

The field of one-dimensional silicon nanostructures has a tremendous technological potential, encompassing such devices as light emitting diodes, field effect transistors, logic gates, and many others. At present, a number of perfect silicon and silicon-silica nanowires of various shapes and effective sizes were synthesized under high temperature conditions.[1–3] All silicon nanowires have hemispherical caps at the end of the structures not connected with the substrate. It was shown[4] that the presence of a quantum dot at the end of nanowire is energetically preferable.

The silicon nanowires reveal a remarkable electronic structure and confine electrons in a special way. The photoluminiscence excitation energies are closely related to the electronic band gap, and the quantum confinement effect (QCE) is the band gap Δ dependence on the maximum linear size d of the species expressed as $\Delta = A + Cd^{-k}$ form, where A, C, and k are the sample-dependent parameters. The QCE of the silicon nanostructures has been studied using both experimental and theoretical techniques.[5–9]

In a recent experimental work,[10] branched and hyperbranched silicon nanowire structures were synthesized with multiple secondary legs, terminated by catalyst droplets. These structures grow at 60° (or 120°) angle with respect to the silicon nanowire backbone, also terminated by a catalyst droplet. The 60°/120° angles between the legs and backbone exactly match the theoretical models,[4] where the formation of such kind of complex nanostructures relies upon local structural variations of the backbone such as the insertion of a fragment of a different structure type into the nanowire atomic lattice. Because of the structural irregularities one can easily expect a breakdown of the perfect one-dimensional periodicity of the branched silicon nanowires[10] affecting the electronic properties of the species.

In contrast to medium or thick nanowires, which reveal square or rectangular cross sections, thin (1.3–7 nm in diameter) silicon nanowires[2,11] have nearly polygonal or round cross sections. Some of them have the [110] main axis with (100) facets.[11] Theoretical models of the atomic structure of pentagonal and hexagonal nanowires with the main [110] axis and five or six (100) facets, respectively, were proposed.[12] The nanowires of both types have a central pentagonal/hexagonal prism as the core, surrounded by several layers of the hexagonal prisms; they show a pronounced segment structure [Fig. 1(a)].

The pentagonal silicon nanowires described above can be called $P^{m}_{100}(n)$, where P denotes the pentagonal central core, surrounded by $m-1$ hexagonal prism layers along the [110] direction with (100) facets, and n is the number of segments [Fig. 1(a)]. All (100) facets permit low-energy reconstruction with formation of dimer-row patterns perpendicular to the nanowire's main axis decreasing their surface.[12,13] To reflect the dimer surface reconstruction an additional asterisk symbol [$P^{m}_{100*}(n)$] is added into the notation. Only nanowires with even n numbers can form regular dimer-row patterns perpendicular to the main axis, while ones with odd n reveal structural distortions during dimer formation. So, through the present work we studied $P^{2}_{100*}(n)$ and $P^{3}_{100}(n)$ systems.

Another example of complex silicon nanostructures designed using several silicon crystal units are Goldberg-type quantum dots[14] including icosahedral quantum dots[15] [Fig. 1(b)]. The icosahedral dots were designed by connecting 20

a)Author to whom correspondence should be addressed. Electronic mail: avramov.pavel@fx2.ecs.kyoto-u.ac.jp.

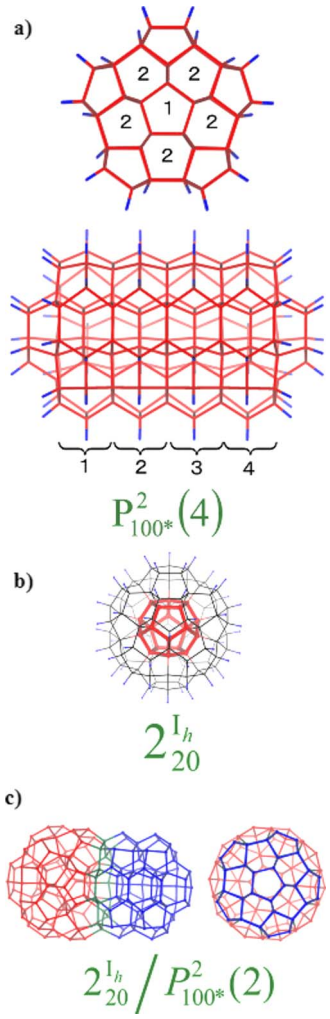

FIG. 1. (Color online) (a) Atomic structure of $P^m_{100*}(n)$ silicon nanowires, illustrated for $m=2$ and $n=4$. m describes the number of prism layers in the nanowire cross section (1 and 2). n gives the number of the lengthwise segments (1, 2, 3, and 4). The asterisk denotes the formation of silicon dimers on the ⟨100⟩ facets of the nanowires. (b) Quantum dot $2^{I_h}_{20}$ with the 20-atom core of I_h symmetry (shown in red sticks). $l=2$ is the number of layers of silicon atoms including the Si_{20} core. (c) Side and top views of the quantum dot attached to the nanowire $2^{I_h}_{20}/P^2_{100*}(2)$. The silicon atoms of the quantum dot, nanowire and the shared interface are shown in red (gray off line), blue (black off line), and green (light gray off line), respectively. Hydrogen atoms are not shown.

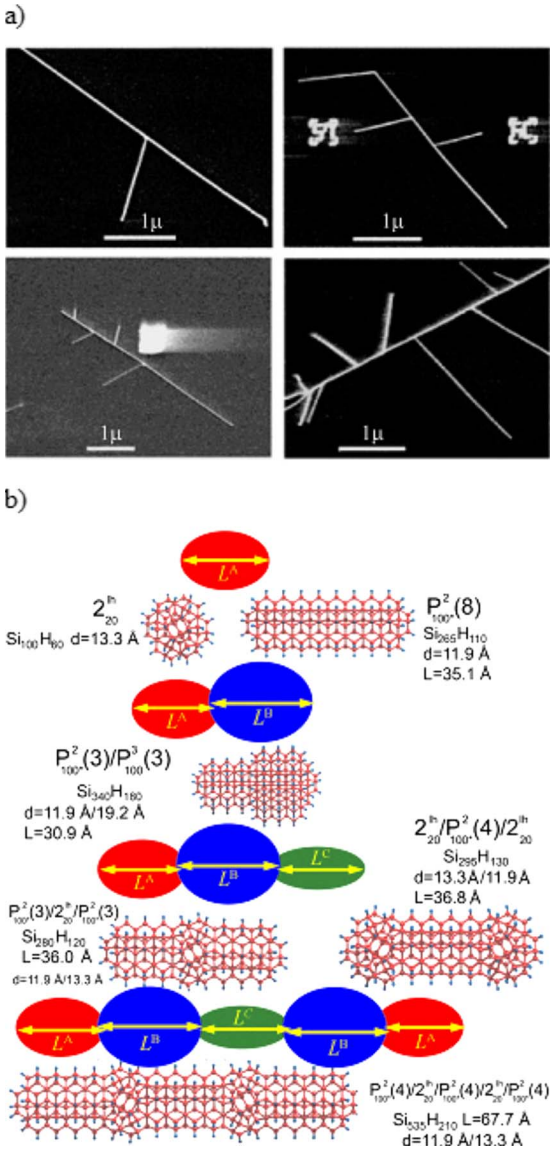

FIG. 2. (Color online) (a) Scanning electron microscopy image of a branched silicon nanowire (adapted from Ref. 10 and reproduced pending the permission from Nano Lett.). b) Atomic structures of silicon nanowires with embedded quantum dots (see main text for the notation). The linear sizes L of the schematic systems (L_A, L_B, L_C) are shown for some actual systems, along with their diameters (d). Only very few of the computed systems are illustrated, and the sizes and symmetry of all systems are provided in Table I. Silicon and hydrogen atoms are shown in red and blue, respectively.

silicon tetrahedrons through three equivalent ⟨111⟩ facets. Twenty silicon atoms located at the center form the central dodecahedron. Depending on the size of the parent tetrahedra, several icosahedral dots with a different number of silicon atoms (Si_{100}, Si_{280}, Si_{600}, Si_{1100}, etc.) can be designed. According to the notation introduced earlier,[14] the icosahedral moiety can be denoted as $l^{I_h}_{20}$, where I_h shows the icosahedral symmetry of the core, the lower index (20) is the number of silicon atoms in it and l is a number of silicon layers including the core. The lowest quantum dot Si_{100} is denoted as $2^{I_h}_{20}$.

Some typical images of branched silicon nanowires[10] are presented in Fig. 2(a). Based on such type of junctions one can design an [110] oriented thin branched pentagonal silicon nanowire with 60° / 120° angles between the legs and the central backbone.[4] Attaching a side branch to such a junction does not considerably deform the atomic structure of the nanowire, and the electronic properties of the branched nanowires can be expected to be largely determined by the backbone and the junction themselves. Experimentally observed nanowires [Fig. 2(a)] have segments of several microns long, and thus appear to be essentially one-dimensional periodic systems with a simple electronic structure. A more interesting behavior with edge effects can be seen in thin nanowires with the linear size on the order of nanometers.

Therefore, motivated by the observed branched structures, we designed silicon nanosystems by adding or inserting quantum dots into nanowires forming quantum dot/nanowire junctions [Figs. 1(c) and 2(b)]. The questions we try to answer in the present theoretical investigation are (a)

what is the atomistic structure of such kind of junctions, and (b) what are the band gaps and other electronic properties of these very interesting objects? Most importantly, how does the branch junctions effect the band gaps and what kind of quantum confinement effect can be observed?

II. CALCULATION TECHNIQUE AND OBJECTS UNDER STUDY

Throughout this work, we used the semiempirical Austin Model 1 (AM1) method[16] based on the modified neglect of diatomic overlap[17] approximation, which was successfully used to study electronic structure of the silicon-based nanoclusters.[10,14] The AM1 approach is generally thought to produce very reasonable geometries, and we used it to fully optimize all structures in this study containing up to about 10^3 silicon atoms. The band gap predicted by AM1 is systematically overestimated by 4.9 eV, reasonably reproducing the quantum confinement effect as determined earlier,[14] therefore, we subtracted this correction from all band gaps reported here.

To study the relationship of the quantum confinement and the linear size of the complex clusters, we designed the complex nanowire/quantum dot junctions using several $l^{I_h}_{20}$, $P^2_{100^*}(n)$, and $P^3_{100}(m)$ parts, as shown in Figs. 1(c) and 2(b). The first type of the complex nanoclusters is $P^2_{100^*}(n)/P^3_{100}(n)$, which is a junction of two nanowires with different diameters (11.9 and 19.2 Å), $n=1,2,\ldots,5$. The second type of complex nanostructures involves one or several quantum dot/nanowire interfaces. We studied the asymmetric $2^{I_h}_{20}/P^2_{100^*}(n)$ $(n=0,1,\ldots,4)$ and $P^2_{100^*}(4)/2^{I_h}_{20}/P^2_{100^*}(n)$ $(n=0,1,\ldots,13)$ as well as symmetric $2^{I_h}_{20}/P^2_{100^*}(n)/2^{I_h}_{20}$ $(n=0,1,\ldots,4)$, $P^2_{100^*}(n)/2^{I_h}_{20}/P^2_{100^*}(n)$ $(n=0,1,\ldots,4)$, and $P^2_{100^*}(4)/2^{I_h}_{20}/P^2_{100^*}(n)/2^{I_h}_{20}/P^2_{100^*}(4)$ $(n=0,1,\ldots,8)$ clusters. Some of the structures are presented in Fig. 2(b).

For the sake of comparison, the electronic structure of a set of pristine $P^2_{100^*}(n_1)$ and $P^3_{100}(n_2)$ $(n_1=1-16,\ n_2=1-8)$ nanowires was also calculated. Their band gaps are presented in Fig. 3(a). The uniform electron delocalization in these structures (see Table I for more details) is the main reason of the narrowing of the band gap under going from small clusters to the bulk semiconductors.[18]

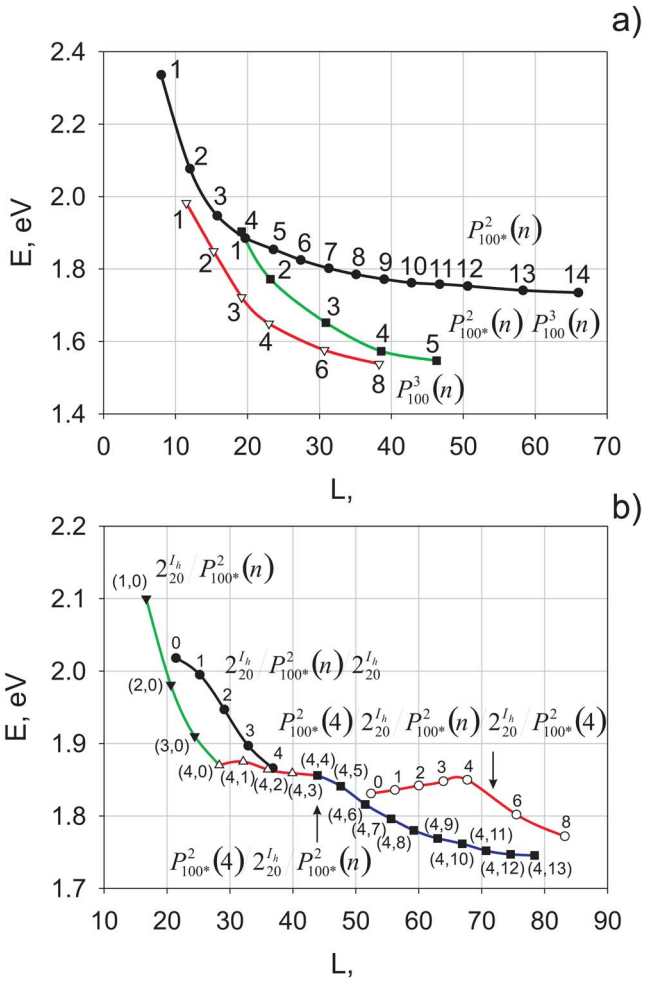

FIG. 3. (Color online) Band gap energy dependence on the linear size L, showing the quantum confinement effect in (a) simple nanowires $P^2_{100^*}(n)$: black lines with circles, $P^3_{100}(n)$: red lines with triangles, and complex connected nanowires $P^2_{100^*}(n)/P^3_{100}(n)$: green lines with squares; (b) quantum dot–nanowire junctions of $2^{I_h}_{20}/P^2_{100^*}(n)$: green lines with triangles, $2^{I_h}_{20}/P^2_{100^*}(n)/2^{I_h}_{20}$: black lines with circles, $P^2_{100^*}(4)/2^{I_h}_{20}/P^2_{100^*}(n)/2^{I_h}_{20}/P^2_{100^*}(4)$: red lines with circles, and $P^2_{100^*}(4)/2^{I_h}_{20}/P^2_{100^*}(n)$: red lines with triangles $(n<4)$ and blue lines with squares $(n\geq 4)$. Numbers show the number of segments n in nanowires. Pairs of numbers are given if more than one nanowire is present, giving the two independent numbers of segments. $(n,0)$ pairs are equivalent to single n and are so shown to elucidate the structure connection.

III. RESULTS AND DISCUSSION

The symmetric $P^2_{100^*}(n)/P^3_{100}(n)$ structures have the following band gaps. For $n=1$, the diameter of the system $L=19.1$ Å is similar to the diameter of $P^3_{100}(1)$, which is incidentally also close to the linear size of $P^2_{100^*}(4)$ $(L=19.7$ Å). Thus, the band gaps of $P^2_{100^*}(4)$ and $P^2_{100^*}(1)/P^3_{100}(1)$ are very close. We note that the band gap in $P^2_{100^*}(n)/P^3_{100}(n)$ resembles that of $P^3_{100}(n)$ shifted by about 0.05–0.1 eV due to the interaction between the two nanowire pieces. All systems reveal the typical $A+Cd^{-k}$ quantum confinement effect [Fig. 3(a)] with some differences in the A, C, and k parameters.

One of the simplest systems of nanowires with embedded quantum dots possessing the mirror symmetry is $2^{I_h}_{20}/P^2_{100^*}(n)/2^{I_h}_{20}$ [Fig. 2(b)]. The length increase leads to a visible change of the QCE [Fig. 3(b)] in comparison to $P^2_{100^*}(n)$ [Fig. 3(a) and Table I]. The quantum dot diameter $(D=13.3$ Å) is larger than the $P^2_{100^*}(n)$ length up to $n=2$. The systems with $n=0,1$, and 2 reveal the strongest quantum dot–nanowire interactions (quantum dot–quantum dot for $n=0$). These interactions change the incline of the QCE dependence for $2^{I_h}_{20}/P^2_{100^*}(n)/2^{I_h}_{20}$ species [Fig. 3(b)] with a noticeable bump around the length of ~25 Å (the bump is observed because for $n=0$ there is no nanowire piece, so that $n=0$ is quantitatively different from $n>0$). For $n>2$ the nanowire linear size and the band gap are determined by $P^2_{100^*}(n)$, restoring the typical QCE [Fig. 3(b)] shifted by about 0.1 eV with respect to the pristine $P^2_{100^*}(n)$ structures due to the quantum dot–nanowire interactions.

Another type of systems with mirror symmetry is D_{5h}

TABLE I. Atomic and electronic structure of complex nanostructures.

System	Length (Å)	Band gap (eV)[a]	ε_{HOMO} (eV)	Symmetry group
$2^{I_h}_{20}/2^{I_h}_{20}$	21.4	2.03	−9.39	D_{5h}
$2^{I_h}_{20}/P^2_{100^*}(1)/2^{I_h}_{20}$	25.2	2.01	−9.36	D_{5h}
$2^{I_h}_{20}/P^2_{100^*}(2)/2^{I_h}_{20}$	29.1	1.96	−9.31	D_{5h}
$2^{I_h}_{20}/P^2_{100^*}(3)/2^{I_h}_{20}$	32.9	1.91	−9.27	D_{5h}
$2^{I_h}_{20}/P^2_{100^*}(4)/2^{I_h}_{20}$	36.8	1.88	−9.25	D_{5h}
$2^{I_h}_{20}/P^2_{100^*}(1)$	16.7	2.11	−9.40	C_{5v}
$2^{I_h}_{20}/P^2_{100^*}(2)$	20.6	1.99	−9.31	C_{5v}
$2^{I_h}_{20}/P^2_{100^*}(3)$	24.4	1.92	−9.26	C_{5v}
$2^{I_h}_{20}/P^2_{100^*}(4)$	28.3	1.88	−9.24	C_{5v}
$P^2_{100^*}(1)/2^{I_h}_{20}/P^2_{100^*}(4)$	32.1	1.89	−9.24	C_{5v}
$P^2_{100^*}(2)/2^{I_h}_{20}/P^2_{100^*}(4)$	36.0	1.87	−9.24	C_{5v}
$P^2_{100^*}(3)/2^{I_h}_{20}/P^2_{100^*}(4)$	39.9	1.86	−9.24	C_{5v}
$P^2_{100^*}(4)/2^{I_h}_{20}/P^2_{100^*}(4)$	43.9	1.86	−9.24	D_{5h}
$P^2_{100^*}(5)/2^{I_h}_{20}/P^2_{100^*}(4)$	47.6	1.85	−9.22	C_{5v}
$P^2_{100^*}(6)/2^{I_h}_{20}/P^2_{100^*}(4)$	51.5	1.83	−9.20	C_{5v}
$P^2_{100^*}(7)/2^{I_h}_{20}/P^2_{100^*}(4)$	55.6	1.81	−9.18	C_{5v}
$P^2_{100^*}(8)/2^{I_h}_{20}/P^2_{100^*}(4)$	59.2	1.79	−9.17	C_{5v}
$P^2_{100^*}(9)/2^{I_h}_{20}/P^2_{100^*}(4)$	63.0	1.78	−9.16	C_{5v}
$P^2_{100^*}(10)/2^{I_h}_{20}/P^2_{100^*}(4)$	66.9	1.77	−9.15	C_{5v}
$P^2_{100^*}(11)/2^{I_h}_{20}/P^2_{100^*}(4)$	70.7	1.76	−9.15	C_{5v}
$P^2_{100^*}(12)/2^{I_h}_{20}/P^2_{100^*}(4)$	74.6	1.75	−9.14	C_{5v}
$P^2_{100^*}(13)/2^{I_h}_{20}/P^2_{100^*}(4)$	78.4	1.75	−9.14	C_{5v}
$P^2_{100^*}(1)/P^3_{100}(1)$	19.2	1.91	−9.21	C_{5v}
$P^2_{100^*}(2)/P^3_{100}(2)$	23.2	1.78	−9.03	C_{5v}
$P^2_{100^*}(3)/P^3_{100}(3)$	30.9	1.66	−8.95	C_{5v}
$P^2_{100^*}(4)/P^3_{100}(4)$	38.6	1.58	−8.89	C_{5v}
$P^2_{100^*}(5)/P^3_{100}(5)$	46.3	1.56	−8.87	C_{5v}
$P^2_{100^*}(4)/2^{I_h}_{20}/2^{I_h}_{20}/P^2_{100^*}(4)$	52.4	1.84	−9.23	D_{5h}
$P^2_{100^*}(4)/2^{I_h}_{20}/P^2_{100^*}(1)/2^{I_h}_{20}/P^2_{100^*}(4)$	56.2	1.84	−9.24	D_{5h}
$P^2_{100^*}(4)/2^{I_h}_{20}/P^2_{100^*}(2)/2^{I_h}_{20}/P^2_{100^*}(4)$	60.0	1.85	−9.24	D_{5h}
$P^2_{100^*}(4)/2^{I_h}_{20}/P^2_{100^*}(3)/2^{I_h}_{20}/P^2_{100^*}(4)$	63.9	1.85	−9.24	D_{5h}
$P^2_{100^*}(4)/2^{I_h}_{20}/P^2_{100^*}(4)/2^{I_h}_{20}/P^2_{100^*}(4)$	67.7	1.86	−9.24	D_{5h}
$P^2_{100^*}(4)/2^{I_h}_{20}/P^2_{100^*}(6)/2^{I_h}_{20}/P^2_{100^*}(4)$	75.5	1.81	−9.19	D_{5h}
$P^2_{100^*}(4)/2^{I_h}_{20}/P^2_{100^*}(8)/2^{I_h}_{20}/P^2_{100^*}(4)$	83.2	1.78	−9.17	D_{5h}
$P^2_{100^*}(1)$	8.0	2.34	−9.45	D_{5h}
$P^2_{100^*}(2)$	12.0	2.08	−9.32	D_{5h}
$P^2_{100^*}(3)$	15.8	1.95	−9.25	D_{5h}
$P^2_{100^*}(4)$	19.7	1.89	−9.23	D_{5h}
$P^2_{100^*}(5)$	23.6	1.86	−9.22	D_{5h}
$P^2_{100^*}(6)$	27.4	1.83	−9.20	D_{5h}
$P^2_{100^*}(7)$	31.3	1.81	−9.18	D_{5h}
$P^2_{100^*}(8)$	35.1	1.79	−9.17	D_{5h}
$P^2_{100^*}(9)$	39.0	1.78	−9.16	D_{5h}
$P^2_{100^*}(10)$	42.8	1.77	−9.16	D_{5h}
$P^2_{100^*}(11)$	46.7	1.76	−9.15	D_{5h}
$P^2_{100^*}(12)$	50.6	1.76	−9.15	D_{5h}
$P^2_{100^*}(14)$	58.3	1.75	−9.14	D_{5h}
$P^3_{100}(1)$	11.5 (19.2)[b]	1.99	−9.17	D_{5h}
$P^3_{100}(2)$	15.3 (19.2)[b]	1.85	−9.07	D_{5h}
$P^3_{100}(3)$	19.2 (19.2)[b]	1.73	−8.95	D_{5h}
$P^3_{100}(4)$	23.0	1.65	−8.88	D_{5h}
$P^3_{100}(6)$	30.7	1.58	−8.81	D_{5h}
$P^3_{100}(8)$	38.3	1.54	−8.77	D_{5h}

[a]The band gaps are given with taking into account the AM1 4.9 eV overestimation.[14]

[b]The length of central $P^2_{100^*}(n)$ part.

[c]Diameter.

$P^2_{100^*}(n)/2^{I_h}_{20}/P^2_{100^*}(n)$ $(n=1-4)$. In comparison with $P^2_{100^*}(n)$ (Table I), the insertion of the $2^{I_h}_{20}$ fragments between the two segments of $P^2_{100^*}(n)$ leads to a blue displacement of the band gap at ~0.1 eV. The band gap of the longest $P^2_{100^*}(4)/2^{I_h}_{20}/P^2_{100^*}(4)$ system ($L=43.9$ Å) is equal to 1.87 eV, which corresponds well to the band gap of pristine $P^2_{100^*}(4)$ (1.90 eV, $L=19.7$ Å).

The band gap of the asymmetric $2^{I_h}_{20}/P^2_{100^*}(n)$ system shows a monotonic decline of the band gap determined by the nanowire part, with considerable shifts (0.24–0.10 eV, Table I) for $n=1$ and 2 due to the interaction of the $2^{I_h}_{20}$ and $P^2_{100^*}(n)$ fragments, which have a similar size (~12–13 Å) and thus a similar electronic structure.

A different, nonmonotonic type of the quantum confinement effect is observed in $P^2_{100^*}(4)/2^{I_h}_{20}/P^2_{100^*}(n)$ $(n=0-13)$ and $P^2_{100^*}(4)/2^{I_h}_{20}/P^2_{100^*}(n)/2^{I_h}_{20}/P^2_{100^*}(4)$ $(n=0-8)$. For the former, one can see a plateau in the region of $n=0-4$, and for the latter a maximum near $n=4$ can be observed [Fig. 3(b)]. The plateau is easy to understand, as the band gap is determined largely by the longest nanowire piece, which is fixed for the left nanowire fragment. Small fluctuations in the band gap correspond to some variations in the quantum nanodot–nanowire interactions.

The pentamer system made of two quantum dots and three nanowire segments is perhaps the most unusual one of all in this study. The incline is positive (for $n=0-4$), thus the band gap increases with the system size, which is strikingly contrary to any other system. It is necessary to note that such type of QCE response was observed in an experiment[19] related to the formation of potential barriers between the nanocrystalline silicon fragments in the oxidation process of porous silicon.[20] The origin of this unusual behavior can be seen in the inner nanowire piece $P^2_{100^*}(n)$, which for $n=0-4$ is apparently small enough to influence the electronic states of the terminal nanowire pieces $P^2_{100^*}(4)$, which determine the band gap. The band gap increase over $n=0-4$ does not exceed 0.02 eV, so this is not a large effect. As n grows larger than 4, the band gap is determined by the longest central piece $P^2_{100^*}(n)$ and differs slightly from the band gap in the standalone nanowire of the same size n (e.g., for $n=6$, 1.81, and 1.82 eV) (Table I).

Summarizing, we observe that the quantum confinement is determined by the linear size of the largest constituting unit in the system shifted by the interaction with quantum dots. For instance, in the case of three units (Fig. 2), the band gap is given by $\max(L_A, L_B, L_C)$, and not the total size $L_A+L_B+L_C$; thus, the embedded quantum dots effectively partition the nanowires into separate boxes in which electrons are confined. This shift due to quantum dots is the largest (up to 0.3 eV) for small nanowires ($n<3$), becomes about 0.1 for medium sized systems ($n=3,4$) and turns into nearly zero for larger nanowires. In one case the shift leads to an inverse quantum confinement effect with a maximum.

To illustrate and further substantiate the above conclusions, the total and partial densities of states (DOSs) are shown in Fig. 4. The partial DOSs were calculated by taking the electron density due to the atomic orbitals centered at specific pieces of the systems. The Gaussian broadening of

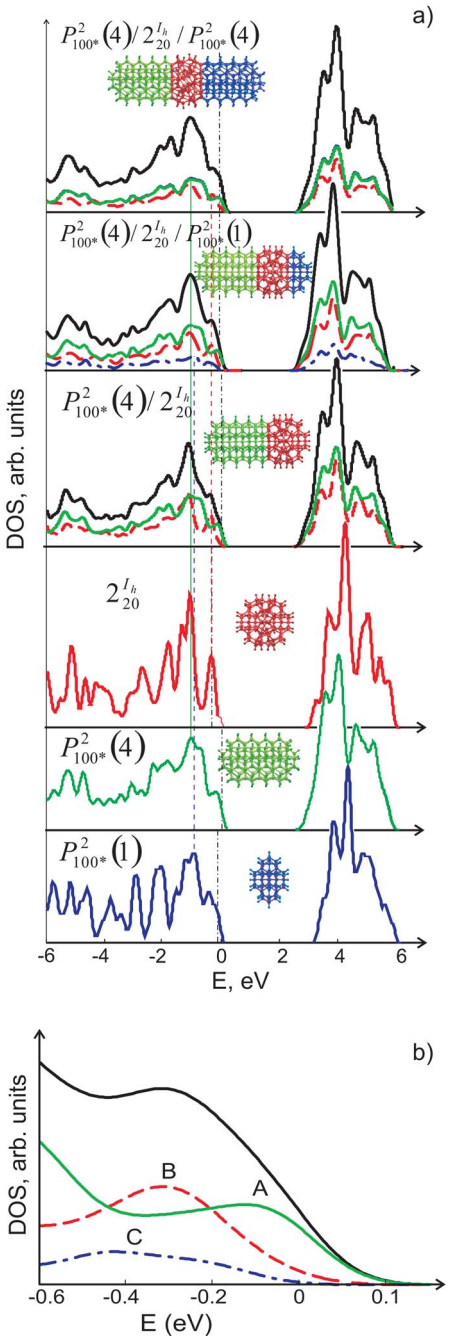

FIG. 4. (Color online) (a) Total and partial DOS of complex nanoclusters. Partial DOS are shown in the same color as the corresponding atomic structures. (b) The detailed total and partial DOS of occupied electronic states of $P^2_{100^*}(4)/2^{I_h}_{20}/P^2_{100^*}(1)$ cluster near the Fermi level region. Peaks *A*, *B*, and *C* correspond to the $P^2_{100^*}(4)$, $2^{I_h}_{20}$, and $P^2_{100^*}(1)$ fragments respectively.

all DOS curves throughout the whole Fig. 4 is equal to 0.1 eV. The highest occupied molecular orbital (HOMO) level of $P^2_{100^*}(4)/2^{I_h}_{20}/P^2_{100^*}(4)$ cluster has been chosen as the zero energy and the total densities of other structures were shifted along the *x* axis to align the positions of the main maxima with this reference DOS. All vacant states were uniformly shifted by 4.9 eV toward the occupied ones. The analysis of DOS is useful to discuss the role of orbital interactions in the formation of complex structures.[21,22]

The total DOS shapes of $P^2_{100^*}(1)$ and $P^2_{100^*}(4)$ are close to each other and significantly differ from that of $2^{I_h}_{20}$ [Fig. 4(a)]. The total DOS of the complex systems such as $P^2_{100^*}(4)/2^{I_h}_{20}/P^2_{100^*}(4)$ appear to be essentially additive of the corresponding constituting pieces. The atomic orbitals at the interface mix with each other, and one can see some broadening of the partial densities compared to the independent pieces, which in turn reduces the effective partial band gap between the occupied and virtual zones.

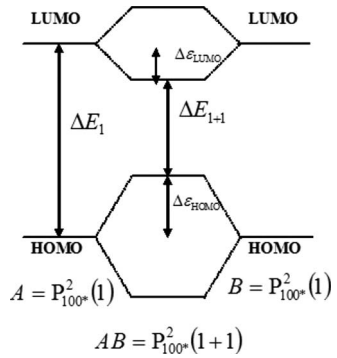

FIG. 5. Molecular orbital diagram elucidating the quantum confinement. When system $A=P^2_{100^*}(1)$ is elongated with $B=P^2_{100^*}(1)$ producing $AB=P^2_{100^*}(2)$, nearly degenerate occupied and virtual orbitals are shifted by the $A-B$ interaction (e.g., the HOMO and LUMO orbital energies shifted by $\Delta\varepsilon_{HOMO}$ and $\Delta\varepsilon_{LUMO}$, respectively), reducing the band gap from ΔE_1 to ΔE_{1+1}.

A typical example of the partial DOS interactions near the Fermi region in Fig. 4(a) is shown enlarged in Fig. 4(b) for $P^2_{100^*}(4)/2^{I_h}_{20}/P^2_{100^*}(1)$ cluster. The peak *A* [of $P^2_{100^*}(4)$] is the highest in energy (−0.05 eV). The peaks *B* [$P^2_{100^*}(1)$] and *C* ($2^{I_h}_{20}$) at −0.3 and −0.4 eV, respectively, are located lower in energy in the same region and form the main *B*+*C* peak of the total DOS. Peaks *B* and *C* are close in energy and the corresponding electronic states interact strongly, which is related to the similarity in the linear sizes of $P^2_{100^*}(1)$ and $2^{I_h}_{20}$: 6.12 and 9.0 Å, respectively. The other $P^2_{100^*}(4)$ piece (peak *A*) has a significantly bigger length (17.8 Å) and thus interacts weakly with $P^2_{100^*}(1)$ and $2^{I_h}_{20}$. The band gap of $P^2_{100^*}(4)/2^{I_h}_{20}/P^2_{100^*}(1)$ is determined by $P^2_{100^*}(4)$ (peak *A*), which forms the HOMO region.

In the regions away from the Fermi level [Fig. 4(a)], at the energy of about −1 eV or less, the occupied electronic states centered at different parts are strongly mixed due to the interactions with each other and determine electronic states delocalized through the whole complex nanostructure. The vacant zones of pieces, in general, are closer to each other and thus interact stronger than the occupied zones.

A schematic with a simple molecular orbital explanation of the quantum confinement effect (Fig. 5) is provided. When one elongates a nanowire, e.g., from $P^2_{100^*}(1)$ by adding another segment $P^2_{100^*}(1)$, the degenerate HOMO and lowest unoccupied molecular orbital (LUMO) of the two pieces are shifted because of the interaction between the fragments. If a quantum dot is embedded in nanowire [e.g., $P^2_{100^*}(n)/2^{I_h}_{20}/P^2_{100^*}(1)$], then the orbitals of the two nanowire pieces become separated in space, thus making the interaction nearly zero, and the band gap of the total system resembles that of the independent pieces with some small shift.

As it was shown in Fig. 4(b), there are some interactions

between the quantum dot and nanowire orbitals, but they are weaker and not coherent compared to the nanowrire elongation. The shift of the HOMO (LUMO) levels of $P^2_{100^*}(1)$ and $2^{I_h}_{20}$ is equal to 0.1 eV, whereas for the $P^2_{100^*}(4)$ and $2^{I_h}_{20}$ pair it is significantly greater: 0.3 (0.1) eV. Thus, the interactions between the two electronic subsystems in the latter case are smaller than that in the former.

IV. CONCLUSIONS

Silicon quantum dots embedded into nanowires effectively partition the quantum confinement, and the band gap is determined by the longest nanowire piece of the system. The typical $1/d$ dependence of the band gap upon the total system size is destroyed in some cases, with an observed plateau and a maximum corresponding to the inverse quantum confinement effect. The formation of the interfaces between the constituting parts leads to the interactions of their electronic subsystems, which are stronger for the Fermi level regions if the pieces are of a similar electronic structure (i.e., are of a similar size). The proposed theoretical analysis can be used to interpret crucial experimental data for branched nanosystems.

ACKNOWLEDGMENTS

This work was, in part, partially supported by a Core Research for Evolutional Science and Technology (CREST) grant in the area of high performance computing for multiscale and multiphysics phenomena from the Japan Science and Technology Agency (JST) as well as by the Russian Fund of Basic Researches (Grant No. 05-02-17443) (L.A.C.). One of the authors (P.V.A.) acknowledges the encouragement of Dr. Keiji Morokuma, Research Leader at Fukui Institute. The geometry of all presented structures was visualized by ChemCraft software.[23] L.A.C. acknowledges I. V. Stankevich for help and fruitful discussions. P.B.S. is grateful to the Joint Supercomputer Center of the Russian Academy of Sciences for access to a cluster computer for quantum-chemical calculations.

[1] Y. Wang, V. Schmidt, S. Senz, and U. Gösele, Nat. Nanotechnol. **1**, 186 (2006).
[2] D. Appell, Nature (London) **419**, 553 (2002).
[3] A. M. Morales and C. M. Lieber, Science **279**, 208 (1998).
[4] P. V. Avramov, L. A. Chernozatonskii, P. B. Sorokin, and M. S. Gordon, Nano Lett. **7**, 2063 (2007).
[5] H. Pan, W. Chen, S. H. Lim, C. K. Poh, X. Wu, Y. Feng, W. Ji, and J. Lin, J. Nanosci. Nanotechnol. **5**, 733 (2005).
[6] C. Y. Yeh, S. B. Zhang, and A. Zunger, Phys. Rev. B **50**, 14405 (1994).
[7] A. J. Read, R. J. Needs, K. J. Nash, L. T. Canham, P. D. Calcott, and A. Qteish, Phys. Rev. Lett. **69**, 1232 (1992).
[8] A. M. Saitta, F. Buda, G. Fiumara, and P. V. Giaquinta, Phys. Rev. B **53**, 1446 (1996).
[9] L. L. Wang and A. Zunger, J. Phys. Chem. **98**, 2158 (1994).
[10] D. Wang, F. Qian, C. Yang, Z. Zhong, and C. M. Lieber, Nano Lett. **4**, 871 (2004).
[11] D. D. D. Ma, C. S. Lee, F. C. K. Au, S. Y. Tong, and S. T. Lee, Science **299**, 1874 (2003).
[12] Y. Zhao and B. Yakobson, Phys. Rev. Lett. **91**, 035501 (2003).
[13] P. V. Avramov, A. A. Kuzubov, A. S. Fedorov, P. B. Sorokin, F. N. Tomilin, and Y. Maeda, Phys. Rev. B **75**, 205427 (2007).
[14] P. V. Avramov, D. G. Fedorov, P. B. Sorokin, L. A. Chernozatonskii, and M. S. Gordon, J. Phys. Chem. C **111**, 18824 (2007).
[15] Y. Zhao, Y.-H. Kim, M.-H. Du, and S. B. Zhang, Phys. Rev. Lett. **93**, 015502 (2004).
[16] M. J. S. Dewar, E. G. Zoeblish, E. F. Healyand, and J. J. P. Stewart, J. Am. Chem. Soc. **107**, 3902 (1985).
[17] J. J. P. Stewart, J. Comput. Chem. **10**, 209 (1989).
[18] Al. L. Efros and A. L. Efros, Sov. Phys. Semicond. **16**, 772 (1982).
[19] M. V. Wolkin, J. Jorne, P. M. Fauchet, G. Allan, and C. Delerue, Phys. Rev. Lett. **82**, 197 (1999).
[20] Q. Chen, X.-J. Li, S. Zhang, J. Zhu, G. Zhou, K. Q. Ruan, and Y. Zhang, J. Phys.: Condens. Matter **9**, L569 (1997).
[21] P. V. Avramov and S. G. Ovchinnikov, Zh. Strukt. Khim. **40**, 131 (1999).
[22] P. V. Avramov and S. G. Ovchinnikov, Phys. Solid State **42**, 788 (2000).
[23] The ChemCraft software http://www.chemcraftprog.com has been used for visualization of all structures..